
Practical limits on Nanosatellite Telescope Pointing: The Impact of Disturbances and Photon Noise

Ewan S. Douglas^{1,*}, Kevin Tracy² and Zachary Manchester²

¹ *Department of Astronomy/Steward Observatory, 933 North Cherry Avenue, Rm. N204, Tucson, AZ 85721-0065*

² *The Robotics Institute, Carnegie Mellon University, 5000 Forbes Ave, Pittsburgh, PA 15213*

Correspondence*:
Corresponding Author
douglae@arizona.edu

ABSTRACT

Accurate and stable spacecraft pointing is a requirement of many astronomical observations. Pointing particularly challenges nanosatellites because of an unfavorable surface area to mass ratio and proportionally large volume required for even the smallest attitude control systems. This work explores the limitations on astrophysical attitude knowledge and control in a regime unrestricted by actuator precision or actuator-induced disturbances such as jitter. The external disturbances on an archetypal 6U CubeSat are modeled and the limiting sensing knowledge is calculated from the available stellar flux and grasp of a telescope within the available volume. These inputs are integrated using a model-predictive control scheme. For a simple test case at 1 Hz, with an 85 mm telescope and a single 11th magnitude star, the achievable body pointing is predicted to be 0.39 arcseconds. For a more general limit, integrating available star light, the achievable attitude sensing is approximately 1 milliarcsecond, which leads to a predicted body pointing accuracy of 20 milliarcseconds after application of the control model. These results show significant room for attitude sensing and control systems to improve before astrophysical and environmental limits are reached.

Keywords: attitude sensing and control, environmental disturbances, CubeSats, astrophysics

1 INTRODUCTION

Astronomical observation with nanosatellites requires a level of precision that far exceeds what is capable from common attitude determination and control systems (ADCSs) present on Earth-imaging CubeSats. Note that this work will refer to nanosatellites in an inclusive sense for any spacecraft approximately 10 kg or below, or those that are designed specifically to a CubeSat deployer standard (<https://www.cubesat.org>). Since astronomical light sources are dim and relatively static, these fine-pointing nanosatellites need to observe continuously, or “stare”, for minutes to hours (e.g. Weiss et al. (2014); Shkolnik (2018); Knapp et al. (2020a)). An ideal astronomical ADCS would achieve this by slewing the nanosatellite to the target attitude, and maintaining perfect inertial pointing indefinitely while rejecting transient disturbances that fall below the sampling accuracy of the instrument. Improving nanosatellite pointing enables a range of applications beyond the transformative photometry recently demonstrated by the ASTERIA mission Knapp et al. (2020b). These applications span from direct exoplanet detection by

interferometry (Dandumont et al., 2020) or starshades (Macintosh et al., 2019), to X-rays (Krizmanic et al., 2020), and the ultraviolet (Shkolnik, 2018).

Actuating the attitude of a spacecraft requires application of a torque on the body of the spacecraft. In early nanosatellites this was achieved with onboard magnetorquers interacting with the Earth's magnetic field, allowing for coarse aiming of solar panels and antenna. Miniaturization and implementation of reaction wheels, flywheels spun continuously using precision motors at tens to thousands of revolutions per minute, on these nanosatellites has enabled sub-1 arcminute nanosatellite pointing (Sinclair et al., 2007; Mason et al., 2016).

The attitude control performance of nanosatellites is limited by an unfavorable mass-to-surface-area ratio of both the spacecraft and the small reaction wheels, increasing sensitivity to external disturbances and internal imbalances. While these actuators have proven capable of fine pointing on larger spacecraft, they do not scale down well to smaller spacecraft, as demonstrated in Fig. 1. State-of-the-art reaction wheels allow for precise pointing and rejection of slowly changing disturbances, e.g. drag differentials, but imperfections in the reaction wheels can directly add uncontrolled jitter and excite spacecraft structural modes (Shields et al., 2017; Addari et al., 2017). Thermal drifts and misalignment between attitude sensor star-trackers and science payloads can be addressed when using the science telescope for attitude determination, but the higher-order jitter remains, e.g. analysis in Smith et al. (2010); Nguyen et al. (2018).

Large spacecraft often use control-moment gyros for attitude control, but their increased Size, Weight, and Power (SWaP) and complexity make them impractical for most nanosatellites (Votel and Sinclair, 2012). Spacecraft like the largest NASA observatories are able to achieve the most exquisite pointing via passive damping of these actuators. This damping comes at the cost of significant mass and volume, and becomes more difficult as spacecraft mass decreases. Using great observatories as examples, HST uses viscous dampers (Davis and et al., 1986), each Chandra reaction wheel is isolated by six damping springs arranged in a hexapodal configuration (Pendergast and Schauwecker, 1998), and JWST uses dual stage passive isolation (Bronowicki, 2006). This simple, but fundamental trade between pointing accuracy and SWaP is a major barrier to astrophysics with nanosatellites.

Many proposed solutions to the attitude control limitations of CubeSats have been in the form of second-stage correction (Beierle et al., 2018; Pong, 2018; Cahoy et al., 2019). ASTERIA (Arcsecond Space Telescope Enabling Research in Astrophysics) is the first sub-arcsecond imaging CubeSat (Pong, 2018). The correction was accomplished by image-plane stabilization using a detector-shifting lead zirconate titanate (PZT) stage. The science telescope on ASTERIA operates at 20 Hz, reading out 50 ms exposures for science and pointing control, limiting the detectable stellar magnitude to $m_V < 7$ since dimmer stars do not flip the detector's first analog-to-digital bit (Knapp et al., 2020a) in an exposure. Similarly, the CLICK free-space laser communications CubeSats (Cahoy et al., 2019), due for launch in 2021, will use microelectromechanical systems (MEMS)-based steering mirrors to achieve fine pointing while the DeMi mission launched in 2020 is designed to use a MEMS deformable mirror for fine wavefront steering (Morgan et al., 2019).

The combination of controller bandwidth and photon noise from stars presents a fundamental limit to attitude control with reaction wheels. Without a large aperture and corresponding large number of photons per exposure, photoelectron shot noise limits the centroid accuracy of the star tracker or astronomical telescope. As a Poisson process, error is proportional to the square root of the number of photoelectrons per exposure; thus, for a simple disturbance environment the achievable pointing decreases linearly with telescope diameter. Unfortunately, performance degrades faster than this in practice. Crossing a structural

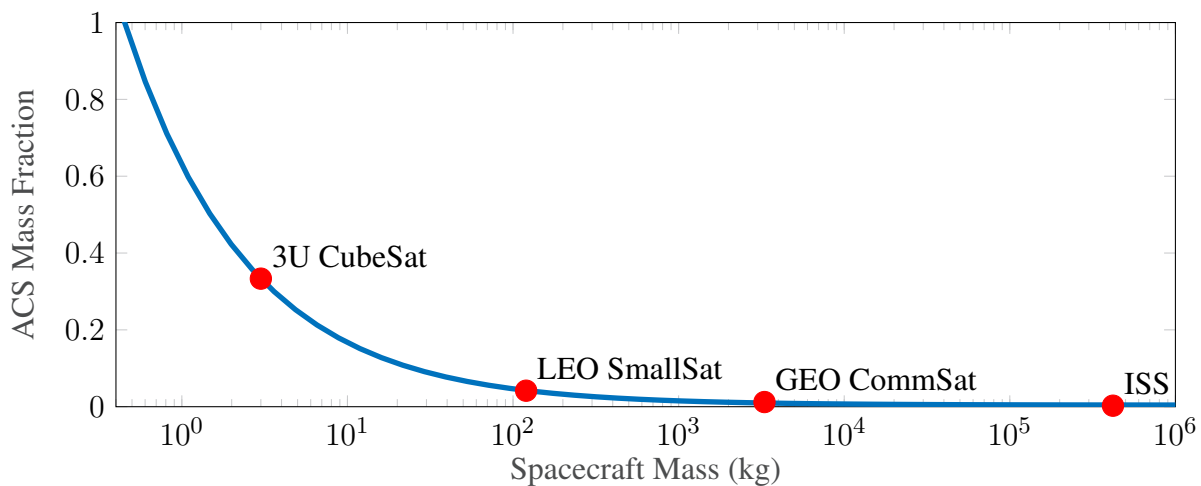


Figure 1. Approximate mass fraction consumed by momentum actuators as a function of spacecraft mass.

mode of the spacecraft can have devastating impacts on stability, and manufacturing tolerance limits mean reaction wheel imbalances are an even larger fraction of the spacecraft inertia on nanosatellites, so higher bandwidths may be required when fewer photons are available. This work seeks to define the sensing and control limits of satellite pointing, establishing the lower limit *without* considering the limitations imposed by actuators. Actuator-disturbances are usually so dominant that environmental disturbances are entirely neglected in spacecraft design (e.g. Choueiri et al. (2018)).

The two-stage actuator approach is limited for several reasons: pointing correction stages add mass, power, complexity, and risk, not all astronomical optical layouts can accommodate a correction stage, and the bandwidth of the system must be sufficient to correct high-frequency reaction-wheel disturbances. Single-stage approaches that minimize high-frequency noise have also been proposed, including electro-spray thrusters (Mier-Hicks and Lozano, 2017), viscously damped reaction wheels (Underwood et al., 2015), and predictive magnetorquers (Gatherer and Manchester, 2018). While both approaches have various limitations in their actuation precision and dynamic range, they hold great promise. However, we find it imperative to assess the possible gains of these approaches by finding the fundamental limits placed by the input disturbances and sensing available on a nanosatellite platform. This provides a context and methodology

| Symbol | Variable | Notes/values |
|-----------|---|-----------------------------|
| D_x | Sensing Aperture Diameter | variable |
| R_N | Detector Read Noise | $2.6 e^-$, (Micron, 2006) |
| D_N | Detector Dark Noise | $25 e^-/s$, (Micron, 2006) |
| λ | Sensing wavelength | 550 nm |
| BW | Sensing bandwidth | 100 nm |
| τ | effective quantum efficiency and throughput | 0.25 |
| N_{pix} | Number of pixels for centroiding | 4 (minimum) |
| f_0 | Zero-mag flux | Johnson V |
| m_l | limiting magnitude | 13 |

Table 1. Nomenclature and assumed values.

for evaluating the limits on new controller technologies. Sec. 2 introduces our disturbance, sensing, and control models. Sec. 3 details the state-estimation framework used in the closed-loop simulations. Sec. 4 presents the resulting spacecraft body pointing as a function of sensor and control limitations. Sec. 5 discusses the impact of these results, comparing them to the limitations faced by current actuators and the goals of future space astronomy missions.

2 METHODS

2.1 Disturbances

Modern attitude control systems rely on flywheel-based momentum actuators like reaction wheels and control-moment gyroscopes. For a constant density, spacecraft inertia scales like the fifth power of spacecraft length, while disturbances like solar pressure, drag, and friction scale with the second power of spacecraft length (surface area). As shown in figure 1, the mass and volume fraction consumed by momentum actuators increases dramatically as the size of the spacecraft shrinks.

This work neglects magnetic torques, which can be large (Inamori et al., 2013), but depend on the fine details of spacecraft design, since both the intrinsic magnetic moment and the dynamic magnetic moment due to on-board currents can be minimized with careful electrical design and spacecraft magnetic cleanliness (e.g. Mehlem (1978); Stern and DeLapp (2004); Junge and Marliani (2011); Belyayev et al. (2016); Lassakeur et al. (2020)).

Figure 2 depicts the frequency content of environmental disturbances acting on a 6U spacecraft in low-Earth orbit. This figure was generated by simulating 1000 Monte-Carlo runs that included drag, solar radiation pressure, and gravity gradient torques (Markley and Crassidis, 2014; Wertz, 1978). The orbits were sampled uniformly from the range of all possible lower-earth orbits with eccentricity less than 0.03, and altitudes between 400 km and 600 km. The simulation epochs were sampled uniformly between 2014 and 2017 to avoid any bias in solar activity or 3rd body perturbations. The line in the figure is the result of the *maximum* RMS torque over all Monte-Carlo runs for each given frequency. Note that the environmental disturbances that the control system must counteract are concentrated in the first few harmonics of the orbital frequency, and lie almost entirely in the range 0.1 to 10 milliHertz.

In addition to poor scaling for small spacecraft, reaction wheels also produce unwanted high-frequency jitter that is often the main source of pointing error on nanosatellites. This jitter is caused by small mass imbalances in the flywheels as they rotate at hundreds of Hertz. Notably, the frequency content of this jitter is several orders of magnitude higher than the environmental disturbances the wheels are supposed to counteract. The overall control loop for the system discussed here is depicted in Fig. 3. Two notable

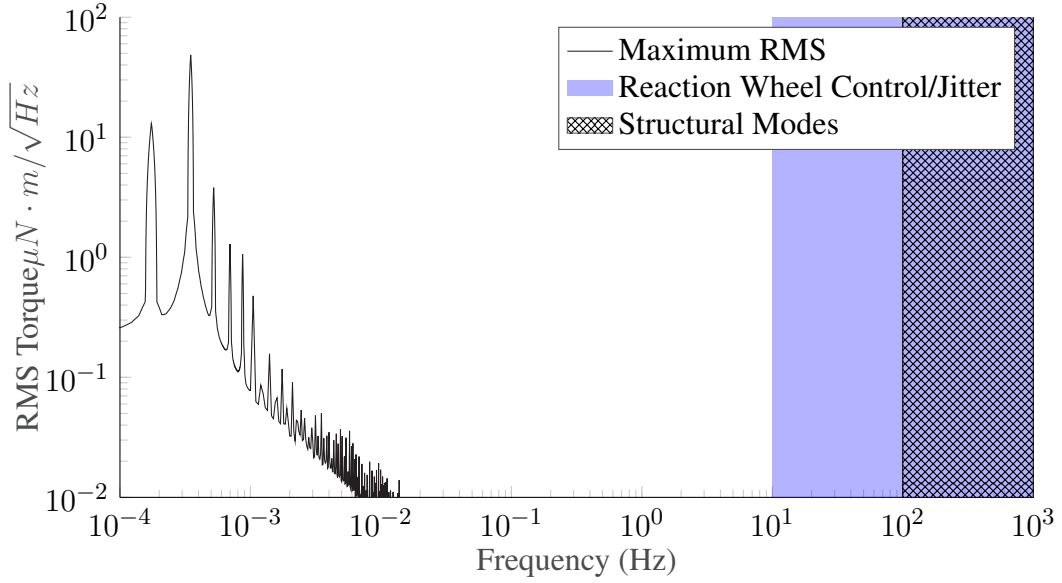


Figure 2. Frequency content of perturbation torques on a small satellite in low-Earth orbit. Disturbances are due to atmospheric drag, solar radiation pressure, and a gravity gradient. The disturbances manifest on the left as solid curve representing the maximum value from an ensemble of orbits drawn from multiple years of credible low-Earth orbits. On the far right, solid shading illustrates typical actuator-induced error frequencies and hatching represents typical nanosatellite structural modes.

features which will be detailed subsequently, are the model-predictive controller and the addition of a telescope sensor to increase sensor precision.

2.2 Control Methodology

To effectively reason about actuator trade-offs and constraints, the control problem will be formulated as a constrained optimization problem and solved online in a model-predictive control (MPC) scheme. Recent advances in algorithm development and microprocessors have enabled state-of-the-art high-performance MPC solvers that can be run on embedded systems such as drones and CubeSats (Howell et al., 2019; Jackson et al., 2021; Tracy and Manchester, 2020). In typical MPC implementations, the problem in Eq. (1) is solved with a horizon of 10-100 time steps at rates between 10 Hz and 1 kHz. While MPC has been in use in industrial applications since the 1980s, its use has historically been limited by the ability to solve the necessary optimization problems at real-time rates on available computing hardware. Thanks to Moore’s law, it has become possible to do this on ever more complicated systems, and today MPC is deployed in a wide range of aerospace and robotics applications, including SpaceX’s autonomous rocket landings (Blackmore, 2016), Boston Dynamics’ humanoid robots (Kuindersma et al., 2016), and autonomous cars (Beal and Gerdes, 2013).

Model-predictive control problems take the general form,

$$\begin{aligned}
 & \underset{x_{1:N}, u_{1:N-1}}{\text{minimize}} && \ell_N(x_N) + \sum_{k=1}^{N-1} \ell_k(x_k, u_k) \\
 & \text{subject to} && x_{k+1} = f(x_k, u_k), \\
 & && g_k(x_k, u_k) \leq 0,
 \end{aligned} \tag{1}$$

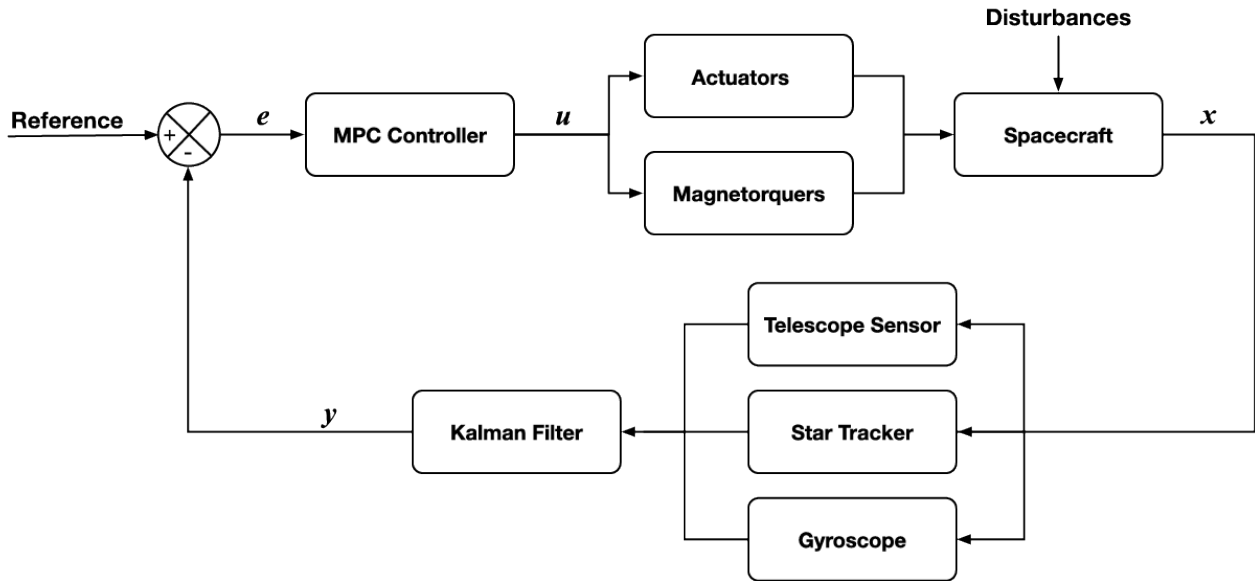


Figure 3. Control system block diagram.

where x_k and u_k are the state and control inputs of the system at time step k , $\ell(x, u)$ is a cost function that penalizes deviations from a desired reference, $f(x, u)$ is a discrete-time dynamics model, and $g(x, u)$ is a set of constraints on the system, including actuator limits and safety constraints. In our case, $f(x, u)$ will encode the attitude dynamics of the spacecraft, the actuators, and the magnetic torque coils, $\ell(x, u)$ will penalize deviations from the desired pointing target, as well as excessive control effort, and $g(x, u)$ will enforce torque limits associated with candidate actuator systems.

2.3 Sensing

Attitude sensing using astronomical sources requires sufficient photon counts to determine direction by accurately measuring a star, or stars', position(s) on a sensor. Here we shall assume an astronomical telescope is included in the nanosatellite payload, either as the primary science instrument, or as an adjuvant co-aligned with another sensor. Various means exist of pulling out attitude knowledge from a telescope and employing a separate science camera, e.g. beamsplitters, dichroics, and field-slicing. We will neglect the details of the implementation except to limit our sensing to a single filter, $BW = 100$ nm, leaving most incoming light available for another specialized science sensor.

In the ideal case, the angular attitude knowledge $\Delta\phi$ perpendicular to an axis (x) depends on the wavelength (λ), and the dimension(s) of the photon collecting aperture, (Δx). As shown by Lindegren (2005), the fundamental pointing error depends on the uncertainty in the momentum of each incident photon. By Heisenberg's uncertainty principle ($\Delta x \Delta p \geq \hbar/2$), the photon's momentum uncertainty (Δp) decreases as uncertainty in the location of the photon increases. Thus, a larger telescope increases Δx and better constrains the angle of the incident photon.

For the case where there are N photons, Lindegren (2013), Eq. 16.1 gives:

$$\Delta\phi = \frac{1}{4\pi} \frac{\lambda}{\Delta x \sqrt{N}}. \quad (2)$$

Where $N = \sigma^2$ is the variance in the photons from Poisson statistics. For a circular aperture diameter D , $\Delta x = D/4$ then

$$\Delta\phi = \frac{1}{\pi} \frac{\lambda}{D_x \sqrt{N}}. \quad (3)$$

The same relation can be derived by assuming a Poisson process and Fraunhofer diffraction (Lindgren, 1978, eq. 32). The number of photons, N , received by the sensor depends on the exposure time and the light grasp or *étendue* of the system. The *étendue* is defined as the product of the collecting area, $\pi(Dx/2)^2$ and the solid-angle, Ω subtended by the instrument. A complicating factor is that the number of stars visible within the collecting area varies with direction on the sky. To calculate the distribution of stars on the sky, we conservatively estimate the differential number of stars per square degree $\mathcal{A}(\text{stars}/\text{mag}/\text{deg}^2)$, where the stellar density is lowest at the galactic poles from (Bahcall and Soneira, 1980, fig 4a). The assumed stellar density versus magnitude is shown in Fig. 4 and is a composite of the Bright Star catalog and the galactic pole estimate. At lower galactic latitudes, stars are more plentiful and more flux would be available than is assumed here, though deleterious effects such as confusion and reddening become more pronounced. The Hipparcos catalog ESA (1997) is shown as a solid orange line for comparison, the integrated sky appearing slightly brighter until the catalog completeness falls off above $m_V \sim 9$. Newer catalogs such as Gaia (Mora et al., 2016) would provide increased precision but not discernibly alter the shape of the stellar density function for these relative bright stars. Neglecting detector effects, integration over the distribution of stellar magnitudes (m) and the instrument field-of-view (FOV) gives the total number of photons per second received by the detector from stars up to a limiting magnitude m_l . Since only four stars in the terrestrial sky are brighter than apparent magnitude zero, we neglect negative magnitudes and the total flux received is

$$\mathcal{F} = \int_{FOV} \int_0^{m_l} \mathcal{A} \tau f_0 10^{-2m/5} d\Omega dm, \quad (4)$$

where f_0 is the zero-point magnitude of the instrument band-pass and τ is the effective throughput including losses due to optics and sensor quantum efficiency.

For our analysis, we assume the spacecraft is sufficiently stable that individual stars can be identified and smearing in a given exposure is negligible. While not discussed here, the length of star smearing can be used to determine the angular rate of the spacecraft (Enright et al., 2010). Attitude sensing using astronomical sources requires sufficient photon counts to accurately determine direction by accurately measuring the star position(s). Fig. 5 shows the sensing limits with (dashed curves) and without the addition of uncertainty due to a low-performance, high-technology readiness level (TRL) detector (dot-dashed curves) described in Section 4.

3 STATE ESTIMATION

In addition to the astronomical telescope, a compact star tracker and gyroscope are included in our model for coarse attitude determination. Typical COTS star trackers for CubeSats provide attitude determination with an accuracy of tens of arcseconds, and are able to maintain tracking at slew rates of several degrees per second. Measurements from all sensors are fused in a multiplicative extended Kalman filter (MEKF) (Lefferts et al., 1982) to calculate a maximum-likelihood estimate of the spacecraft's attitude.

In addition to estimating the attitude of the spacecraft body, parameterized by quaternion q , the filter also estimates a gyroscope bias vector b , an external bias torque τ , and the time derivative of this external torque $\dot{\tau}$. We assume that the environmental disturbances vary slowly compared to the filter update rate, making a first-order process model sufficiently accurate. Both the gyro bias, as well as the derivative of the

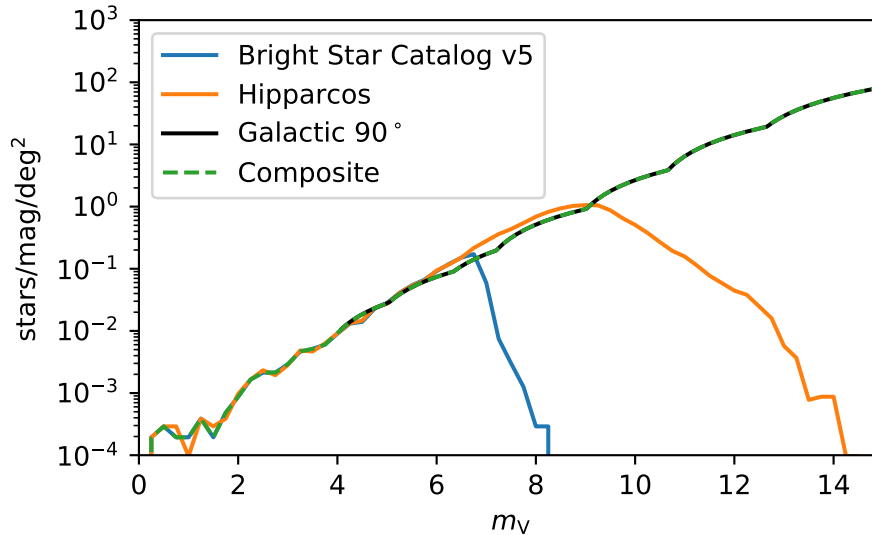


Figure 4. Star counts in units of stellar density per magnitude and per square degree. The dashed curve represents the density used in this work and represents a composite of the Bright Star Catalog (Hoffleit D., 1991) for bright stars and the galactic pole curve from Bahcall and Soneira (1980) at dimmer magnitudes provides a lower limit on stellar density by assuming observations are of the sparsest region of the sky. This composite represents a conservative estimate of the number photons available to localize spacecraft attitude control.

external torque, are assumed to follow a random walk process, while the gyroscope measurements ω are assumed to be corrupted by additive white Gaussian noise. The MEKF process model is,

$$\dot{x}_{kf} = \begin{bmatrix} \dot{q} \\ \dot{b} \\ \dot{\tau} \\ \dot{\tau} \end{bmatrix} = \begin{bmatrix} \frac{1}{2}q \otimes (\omega + \nu_\omega) \\ \nu_b \\ \dot{\tau} \\ \nu_{\dot{\tau}} \end{bmatrix}, \quad (5)$$

where ν_ω , ν_b , and $\nu_{\dot{\tau}}$ are noise inputs drawn from multivariate Gaussian distributions. The covariances $V_{\omega\omega}$ and V_{bb} corresponding to the noise terms ν_ω and ν_b are properties of the gyroscope used, while $V_{\dot{\tau}\dot{\tau}}$ corresponding to $\nu_{\dot{\tau}}$ is calculated based on the expected environmental disturbance torques. The MEKF measurement model, which maps the state x_{kf} into the expected sensor measurements y , is similarly given by,

$$y = h(x_{kf}) + w, \quad (6)$$

where the function $h(x)$ returns expected star locations in the sensor frames based on the current spacecraft state and w is assumed to be drawn from a multivariate Gaussian distribution with covariance matrix W calculated based on Fig. 6.

4 RESULTS

Fig. 6 shows, for example, a single $m_V = 11$ guide star can provide sub-0.1'' pointing knowledge to a 1 Hz sampling system, assuming typical detector noise levels in Table 1 to the calculation of σ . The noise characteristics assumed approximate the MT9P031 complementary metal-oxide-semiconductor (CMOS) sensor with $2.2\mu\text{m}$ pixels, commonly used for precision nanosatellite applications (Becker et al., 2008; Enright et al., 2012; Allan et al., 2018). $m_V = 11$ was chosen because they are common, $\gg 1/\text{star sq. deg}$

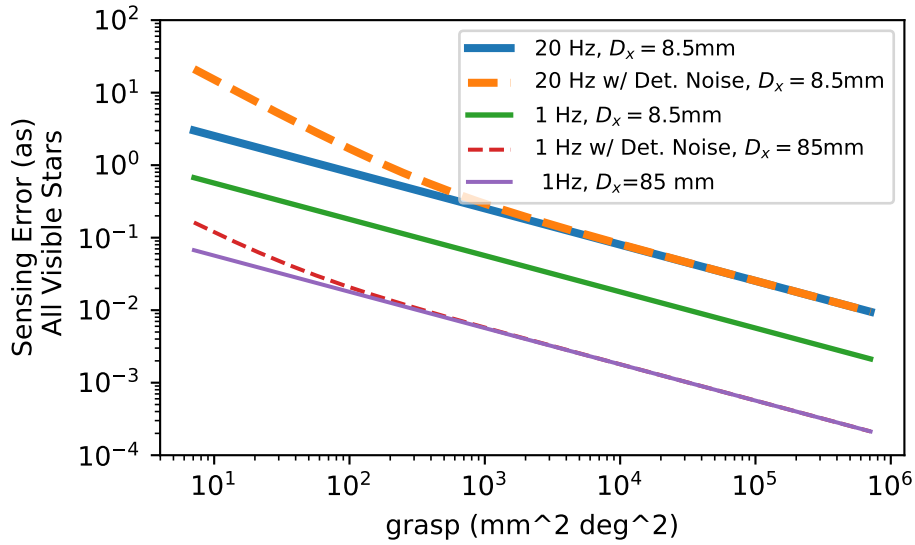


Figure 5. Attitude determination error versus system grasp or *étendue*. This photon noise limited case assumes the flux per square degree at the galactic poles for stars from zero to 13th magnitude, (Fig. 4). The upper bound on the x-axis corresponds to a 85mm diameter telescope with a ten degree circular FOV. The 20 Hz curve is shown to emphasize the importance of short exposure times. At low grasps the detector noise, dominates while, at large grasps, the photon noise dominates. Small values of D_x show the importance of sensor aperture to constraining body pointing, note the largest grasps are likely require an impractically large FOV for $D_x=8.5\text{mm}$.

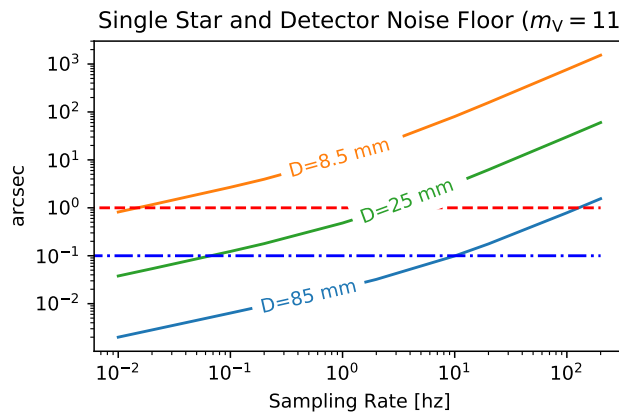


Figure 6. Attitude sensing limit curves assuming centroiding noise due to photon statistics and detector noise from the TRL-9 MT9P031 CMOS detectors widely used on nanosatellites. For an 85 mm space telescope, sub-arcsec sensing is readily achieved at 100 Hz sampling or slower rates, implying ~ 10 Hz bandwidth controllers are as fast as is feasible on dim stars.

on average. Due to the extremely low frequency content of on-orbit environmental disturbances (Fig. 2), the example sampling at 1 Hz is a far higher sample rate than would be needed for an idealized control loop.

Spacecraft body pointing, applying the control system (Fig. 3) to input the disturbances, including photon and sensor noise for a 85 mm telescope observing a single m_V star sampled at 1 Hz is simulated in Fig. 7. This figure shows the time evolution of body pointing for the proposed control system, with a one

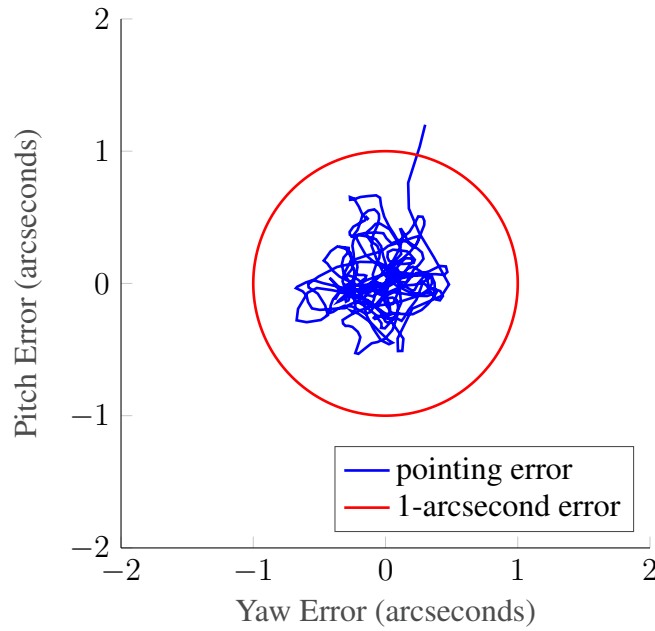


Figure 7. 1 Hz closed-loop control simulation with disturbances from Fig. 2 and sensor noise corresponding to the largest practical telescope that might fit in a 6U CubeSat with an 85 mm diameter, measuring the angle of a single $m_V = 11$ star. The red circle indicates 1 arcsecond error. The initial state is outside the 1 arcsecond circle, but the controller quickly recovers. The resulting RMS body-pointing error is $0.39''$.

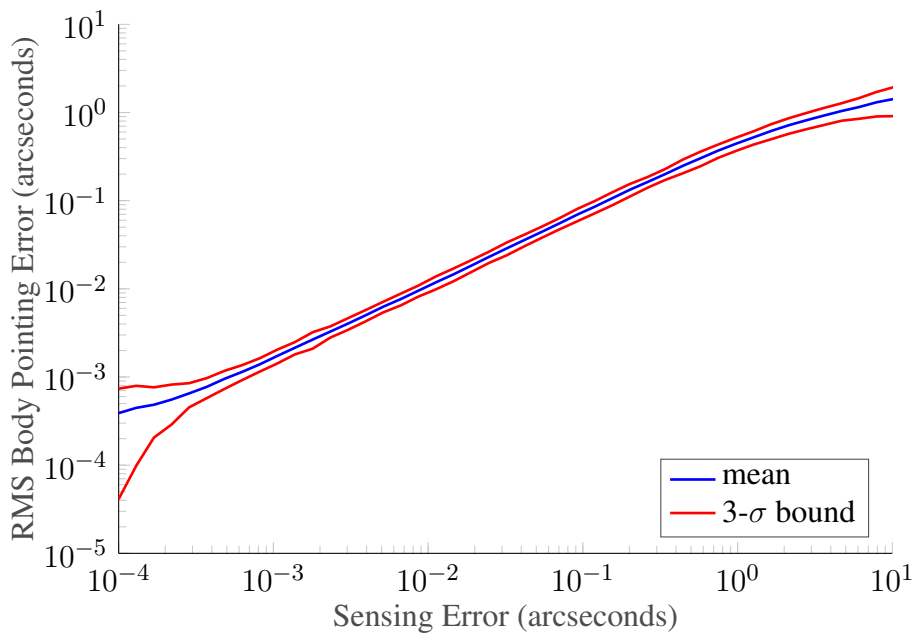


Figure 8. Body pointing RMS error as it relates to sensing error (whether photon or detector limited). Data are from 1000 Monte-Carlo trials with full environmental disturbance torques. Each point on these curves corresponds to a full simulation analogous to that shown in Fig. 7.

arcsecond circle for reference. With the starting point outside the one-arcsecond circle, the body pointing of the reference 6U CubeSat orbit is quickly controlled to an RMS of 0.39 arcseconds.

Fig. 8 extends this analysis to a range of sensing errors. The center line, bracketed by $3 - \sigma$ bounds, shows the RMS body pointing versus absolute sensing error, demonstrating a relationship where the pointing error closely matches the sensing error over a broad range. This is noteworthy since it suggests that the limiting factor in pointing performance comes from the sensing errors instead of jitter induced by the actuators or bandwidth limits in the control system. The sensor grasp or aperture that would reach this level of performance can be found by observing the sensing errors in Fig. 6 or 5. For example, to reach $0.1''$ at 1 Hz using all available starlight, a grasp of $\gtrsim 200 \text{ mm deg}^2$ is needed, while a single 11th magnitude star is insufficient to reach that level in a nanosatellite aperture.

5 CONCLUSIONS

In 1980 Nancy Grace Roman said “pointing has been the pacing team that has really controlled what we’ve been able to do in space astronomy as the field has developed” (Roman and DeVorkin, 1980)¹. This assertion, a “Roman’s Law” for spacecraft capabilities, continues to hold true, and pointing remains a particular challenge for nanosatellites.

Detector dynamic range constraints were neglected in this analysis: Present-day sensors with limited bit depth will not be able to capture all the incident photons without saturating. This limits the useful input flux. Similarly, low noise detectors allow sensing of dimmer stars, changing the brightness cutoff, m_l . Since the brightest stars are also the rarest, this will generally have less impact than might be first assumed, but suggests the importance of both improved actuators and high-dynamic-range sensors and readout electronics for future ADCSs.

Detector pixel sampling was implicitly optimized across this analysis and, for physical designs, the FOV and grasp must be carefully weighed against pixel size and detector noise levels. Caution must be used when applying the sensing-error-versus-grasp curve on Fig. 5 to constrain physical designs. Physical designs must include detector noise, pixel sampling values, and centroiding precision. With sufficient flux rates, increasing detector noise by defocusing stars improves centroiding to millipixel levels (Buffington et al., 1991), but must be balanced with per-pixel noise contributions and confusion limits.

The closed-loop simulation results presented here show that the low frequency of environmental disturbances allows for a very slow control loop for inertially pointing spacecraft. While further improvements in estimation and control algorithms are possible, this work demonstrates practical limits of nanosatellite pointing far beyond the current state-of-the-art, and establishes the target for actuator improvements to enable precision astrophysics with nanosatellites.

CONFLICT OF INTEREST STATEMENT

The authors declare that the research was conducted in the absence of any commercial or financial relationships that could be construed as a potential conflict of interest.

AUTHOR CONTRIBUTIONS

E.S.D. led experiment design, simulation, and manuscript preparation. Z.M. led model design, optimization, analysis, and contributed to manuscript preparation. K.T. led disturbance simulations, and contributed to literature review and manuscript preparation.

¹ www.aip.org/history-programs/niels-bohr-library/oral-histories/4846

FUNDING

Portions of this work were supported by the Arizona Board of Regents Technology Research Initiative Fund (TRIF).

ACKNOWLEDGMENTS

The authors thank Laurent Pueyo for many helpful discussions and feedback. This research has made use of the the VizieR catalogue access tool, CDS, Strasbourg, France (DOI : 10.26093/cds/vizieR). The original description of the VizieR service was published in 2000, A&AS 143, 23.

DATA AVAILABILITY STATEMENT

Code to reproduce the figures in this paper is available on <https://github.com/RoboticExplorationLab/FinePointing> and citable and archived by Zenodo (Douglas et al., 2021).

REFERENCES

- Addari, D., Aglietti, G. S., and Remedia, M. (2017). Experimental and numerical investigation of coupled microvibration dynamics for satellite reaction wheels. *Journal of Sound and Vibration* 386, 225–241. doi:10.1016/j.jsv.2016.10.003
- Allan, G., Douglas, E. S., Barnes, D., Egan, M., Furesz, G., Grunwald, W., et al. (2018). The deformable mirror demonstration mission (DeMi) CubeSat: optomechanical design validation and laboratory calibration. In *Proc. SPIE* (International Society for Optics and Photonics), vol. 10698, 1069857
- Bahcall, J. N. and Soneira, R. M. (1980). The universe at faint magnitudes. I-Models for the galaxy and the predicted star counts. *The Astrophysical Journal Supplement Series* 44, 73–110
- Beal, C. E. and Gerdes, J. C. (2013). Model Predictive Control for Vehicle Stabilization at the Limits of Handling. *IEEE Transactions on Control Systems Technology* 21, 1258–1269. doi:10.1109/TCST.2012.2200826
- Becker, H. N., Dolphin, M. D., Thorbourn, D. O., Alexander, J. W., and Salomon, P. M. (2008). *Commercial sensory survey radiation testing progress report* (Pasadena, CA: Jet Propulsion Laboratory, National Aeronautics and Space Administration)
- Beierle, C., D’Amico, S., Macintosh, B., and Norton, A. (2018). Two-stage attitude control for direct imaging of exoplanets with a CubeSat telescope. In *Space Telescopes and Instrumentation 2018: Optical, Infrared, and Millimeter Wave*, eds. H. A. MacEwen, M. Lystrup, G. G. Fazio, N. Batalha, E. C. Tong, and N. Siegler (Austin, United States: SPIE), 69. doi:10.1117/12.2314233
- Belyayev, S., Ivchenko, N., Dudkin, F., and Pronenko, V. (2016). PRACTICAL ANALYSIS AND IMPLEMENTATION OF A LOW MAGNETIC CONTAMINATION CUBESAT PLATFORM. In *The 4S Symposium 2016*
- Blackmore, L. (2016). Autonomous Precision Landing of Space Rockets. *The Bridge* 4, 15–20
- Bronowicki, A. J. (2006). Vibration Isolator for Large Space Telescopes. *Journal of Spacecraft and Rockets* 43, 45–53. doi:10.2514/1.12036
- Buffington, A., Booth, C. H., and Hudson, H. S. (1991). Using image area to control CCD systematic errors in spaceborne photometric and astrometric time-series measurements. *PASP* 103, 685. doi:10.1086/132868
- Cahoy, K., Grenfell, P., Crews, A., Long, M., Serra, P., Nguyen, A., et al. (2019). The CubeSat Laser Infrared Crosslink Mission (CLICK). In *International Conference on Space Optics — ICSO 2018*

- (International Society for Optics and Photonics), vol. 11180, 111800Y. doi:10.1117/12.2535953
- Choueiri, M. N., Bell, M., and Peck, M. A. (2018). Cost-Effective and Readily Manufactured Attitude Determination and Control System for NanoSatellites. In *2018 AIAA/ASCE/AHS/ASC Structures, Structural Dynamics, and Materials Conference* (American Institute of Aeronautics and Astronautics), AIAA SciTech Forum. doi:10.2514/6.2018-0802
- Dandumont, C., Defrère, D., Kammerer, J., Absil, O., Quanz, S. P., and Loicq, J. (2020). Exoplanet detection yield of a space-based Bracewell interferometer from small to medium satellites. *J. Astron. Telesc. Instrum. Syst.* 6. doi:10.1117/1.JATIS.6.3.035004
- Davis, L. P. and et al. (1986). Hubble space telescope reaction wheel assembly vibration isolation system. In *Damping Proceedings* (Las Vegas, NV, USA: FLIGHT DYNAMICS LABORATORY AIR FORCE WRIGHT AERONAUTICAL LABORATORIES), vol. BA-I, 695
- [Dataset] Douglas, E., Manchester, Z., and Tracy, K. (2021). douglase/FinePointing: CubeSat Star Sensor, Disturbance, and Control Sims – initial release. Zenodo. doi:10.5281/zenodo.4499318
- Enright, J., Sinclair, D., and Dzamba, T. (2012). The Things You Can't Ignore: Evolving a Sub-Arcsecond Star Tracker. In *AIAA/USU SmallSat Conference*. vol. SSC12-X-7
- Enright, J., Sinclair, D., Grant, C., McVittie, G., and Dzamba, T. (2010). Towards Star Tracker Only Attitude Estimation. *Small Satellite Conference*
- ESA (1997). The HIPPARCOS and TYCHO catalogues. Astrometric and photometric star catalogues derived from the ESA HIPPARCOS Space Astrometry Mission 1200
- Gatherer, A. and Manchester, Z. (2018). MAGNETORQUER-ONLY ATTITUDE CONTROL OF SMALL SATELLITES USING TRAJECTORY OPTIMIZATION. *Advances in the Astronautical Sciences* AAS 19-927, 14
- Hoffleit D., W. J. W. (1991). VizieR online data catalog: Bright star catalogue, 5th revised ed. , V/50
- Howell, T. A., Jackson, B. E., and Manchester, Z. (2019). ALTRO: A Fast Solver for Constrained Trajectory Optimization. In *IEEE/RSJ International Conference on Intelligent Robots and Systems (IROS)* (Macau, China)
- Inamori, T., Wang, J., Saisutjarit, P., and Nakasuka, S. (2013). Jitter reduction of a reaction wheel by management of angular momentum using magnetic torquers in nano- and micro-satellites. *Advances in Space Research* 52, 222–231. doi:10.1016/j.asr.2013.02.014
- Jackson, B. E., Punnoose, T., Neamati, D., Tracy, K., and Jitosho, R. (2021). ALTRO-C: A Fast Solver for Conic Model-Predictive Control. In *International Conference on Robotics and Automation (ICRA)* (Xi'an, China), 8
- Junge, A. and Marliani, F. (2011). Prediction of DC magnetic fields for magnetic cleanliness on spacecraft. In *2011 IEEE International Symposium on Electromagnetic Compatibility*. 834–839. doi:10.1109/ISEMC.2011.6038424
- Knapp, M., Seager, S., Demory, B.-O., Krishnamurthy, A., Smith, M. W., Pong, C. M., et al. (2020a). Demonstrating high-precision photometry with a CubeSat: ASTERIA observations of 55 Cancri e. *The Astronomical Journal* 160, 23. doi:10.3847/1538-3881/ab8bcc
- Knapp, M., Seager, S., Demory, B.-O., Krishnamurthy, A., Smith, M. W., Pong, C. M., et al. (2020b). Demonstrating High-precision Photometry with a CubeSat: ASTERIA Observations of 55 Cancri e. *AJ* 160, 23. doi:10.3847/1538-3881/ab8bcc
- Krizmanic, J., Shah, N., Harding, A., Calhoun, P., Purves, L., Webster, C., et al. (2020). VTXO: the Virtual Telescope for X-ray Observations. *arXiv:2006.12174 [astro-ph]*
- Kuindersma, S., Deits, R., Fallon, M., Valenzuela, A., Dai, H., Permenter, F., et al. (2016). Optimization-based locomotion planning, estimation, and control design for Atlas. *Autonomous Robots* 40, 429–455.

- doi:10.1007/s10514-015-9479-3
- Lassakeur, A., Underwood, C., Taylor, B., and Duke, R. (2020). Magnetic Cleanliness Program on CubeSats and Nanosatellites for Improved Attitude Stability. *Journal of Aeronautics and Space Technologies* 13, 25–41
- Lefferts, E., Markley, F., and Shuster, M. (1982). Kalman Filtering for Spacecraft Attitude Estimation. *Journal of Guidance, Control, and Dynamics* 5, 417–429. doi:10.2514/3.56190
- Lindgren, L. (1978). Photoelectric astrometry - A comparison of methods for precise image location , 197–217
- Lindgren, L. (2005). The Astrometric Instrument of Gaia: Principles. In *Proceedings of the Gaia Symposium (ESA SP-576)*. Editors: C. Turon, K.S. O’Flaherty, M.A.C. Perryman (Observatoire de Paris-Meudon, 4-7 October 2004.: ESA), vol. 576, 29
- Lindgren, L. (2013). High-accuracy positioning: astrometry. In *Observing Photons in Space: A Guide to Experimental Space Astronomy*, eds. M. C. E. Huber, A. Pauluhn, J. L. Culhane, J. G. Timothy, K. Wilhelm, and A. Zehnder (New York, NY: Springer), ISSI Scientific Report Series. 299–311. doi:10.1007/978-1-4614-7804-1_16
- Macintosh, B., D’Amico, S., Koenig, A., and Madurowicz, A. (2019). Miniature Distributed Occulter Telescope (mDOT): A Concept for a Smallsat Mission to Observe Extrasolar Zodiacal Dust and Exoplanets. *AGU Fall Meeting Abstracts* 43
- Markley, F. L. and Crassidis, J. L. (2014). *Fundamentals of Spacecraft Attitude Determination and Control* (New York, NY: Springer New York). doi:10.1007/978-1-4939-0802-8
- Mason, J., Baumgart, M., Woods, T., Hegel, D., Rogler, B., Stafford, G., et al. (2016). MinXSS CubeSat On-Orbit Performance and the First Flight of the Blue Canyon Technologies XACT 3- axis ADCS. In *AIAA/USU Conference on Small Satellites*
- Mehlem, K. (1978). Multiple magnetic dipole modeling and field prediction of satellites. *IEEE Transactions on Magnetics* 14, 1064–1071. doi:10.1109/TMAG.1978.1059983
- [Dataset] Micron (2006). MT9P031 Image Sensor Product Brief
- Mier-Hicks, F. and Lozano, P. C. (2017). Electrospray Thrusters as Precise Attitude Control Actuators for Small Satellites. *Journal of Guidance, Control, and Dynamics* 40, 642–649. doi:10.2514/1.G000736
- Mora, A., Biermann, M., Bombrun, A., Boyadian, J., Chassat, F., Corberand, P., et al. (2016). Gaia: focus, straylight and basic angle. *arXiv:1608.00045 [astro-ph]* , 99042Ddoi:10.1117/12.2230763
- Morgan, R. E., Douglas, E. S., Allan, G. W., Bierden, P., Chakrabarti, S., Cook, T., et al. (2019). MEMS Deformable Mirrors for Space-Based High-Contrast Imaging. *Micromachines* 10, 366. doi:10.3390/mi10060366
- Nguyen, T., Morgan, E., Vanderspek, R., Levine, A., Kephart, M., Francis, J., et al. (2018). Fine-pointing performance and corresponding photometric precision of the Transiting Exoplanet Survey Satellite. *JATIS* 4, 047001. doi:10.1117/1.JATIS.4.4.047001
- Pendergast, K. J. and Schauwecker, C. J. (1998). Use of a passive reaction wheel jitter isolation system to meet the Advanced X-Ray Astrophysics Facility imaging performance requirements. In *Space Telescopes and Instruments V* (International Society for Optics and Photonics), vol. 3356, 1078–1094. doi:10.1117/12.324508
- Pong, C. (2018). On-Orbit Performance & Operation of the Attitude & Pointing Control Subsystems on ASTERIA. *AIAA/USU Conference on Small Satellites*
- Roman, N. G. and DeVorkin, D. H. (1980). *Oral history interview with Nancy Grace Roman*. AIP Oral Histories (AIP Publishing)

- Shields, J., Pong, C., Lo, K., Jones, L., Mohan, S., Marom, C., et al. (2017). Characterization of CubeSat Reaction Wheel Assemblies. *Journal of Small Satellites* 6, 565–580
- Shkolnik, E. L. (2018). On the verge of an astronomy CubeSat revolution. *Nature Astronomy* 2, 374–378. doi:10.1038/s41550-018-0438-8
- Sinclair, D., Grant, C. C., and Zee, R. (2007). Enabling Reaction Wheel Technology for High Performance Nanosatellite Attitude Control. *AIAA/USU Conference on Small Satellites*
- Smith, M. W., Seager, S., Pong, C. M., Villaseñor, J. S., Ricker, G. R., Miller, D. W., et al. (2010). ExoplanetSat: detecting transiting exoplanets using a low-cost CubeSat platform. In *Proc. SPIE*, eds. J. M. Oschmann, Jr., M. C. Clampin, and H. A. MacEwen. 773127. doi:10.1117/12.856559
- Stern, T. and DeLapp, S. (2004). Techniques for Magnetic Cleanliness on Spacecraft Solar Arrays. In *2nd International Energy Conversion Engineering Conference* (Providence, Rhode Island: American Institute of Aeronautics and Astronautics). doi:10.2514/6.2004-5581
- Tracy, K. and Manchester, Z. (2020). Model-Predictive Attitude Control for Flexible Spacecraft During Thruster Firings. In *AAS/AIAA Astrodynamics Specialist Conference* (Lake Tahoe, CA)
- Underwood, C., Pellegrino, S., Lappas, V. J., Bridges, C. P., and Baker, J. (2015). Using CubeSat/microsatellite technology to demonstrate the Autonomous Assembly of a Reconfigurable Space Telescope (AAReST). *Acta Astronautica* 114, 112–122
- Votel, R. and Sinclair, D. (2012). Comparison of Control Moment Gyros and Reaction Wheels for Small Earth-Observing Satellites. *Small Satellite Conference*
- Weiss, W. W., Rucinski, S. M., Moffat, A. F. J., Schwarzenberg-Czerny, A., Koudelka, O. F., Grant, C. C., et al. (2014). BRITe-Constellation: nanosatellites for precision photometry of bright stars. *Publications of the Astronomical Society of the Pacific* 126, 573–585. doi:10.1086/677236
- Wertz, J. R. (ed.) (1978). *Spacecraft Attitude Determination and Control*, vol. 73 of *Astrophysics and Space Science Library* (Dordrecht: Springer Netherlands). doi:10.1007/978-94-009-9907-7